Detection of Aliphatically Bridged Multi-Core Polycyclic Aromatic Hydrocarbons in Sooting Flames with Atmospheric-Sampling High-Resolution Tandem Mass Spectrometry

B. D. Adamson,[a)] S. A. Skeen,[a)] M. Ahmed,[b)] N. Hansen[a),*]

[a)] *Combustion Research Facility, Sandia National Laboratories, Livermore, CA 94551, USA*

[b)] *Chemical Sciences Division, Lawrence Berkeley National Laboratory, Berkeley, CA 94720, USA*

submitted to

J. Phys. Chem. A

39 Pages

10 Figures

[*] Corresponding author (NH): email: nhansen@sandia.gov; phone: +1 925 294 6272

Abstract

This paper provides experimental evidence for the chemical structures of aliphatically substituted and aliphatically bridged polycyclic aromatic hydrocarbon (PAH) species in the gas-phase of combustion environments. The identification of these single- and multi-core aromatic species, which have been hypothesized to be important in PAH growth and soot nucleation, was made possible through a combination of sampling gaseous constituents from an atmospheric pressure inverse co-flow diffusion flame of ethylene and high-resolution tandem mass spectrometry (MS-MS). In these experiments, the flame-sampled components were ionized using a continuous VUV lamp at 10.0 eV and the ions were subsequently fragmented through collisions with Ar atoms in a collision-induced dissociation (CID) process. The resulting fragment ions, which were separated using a reflectron time-of-flight mass spectrometer, were used to extract structural information about the sampled aromatic compounds. The high-resolution mass spectra revealed the presence of alkylated single-core aromatic compounds and the fragment ions that were observed correspond to the loss of saturated and unsaturated units containing up to a total of 6 carbon atoms. Furthermore, the aromatic structures that form the foundational building blocks of the larger PAHs were identified to be smaller single-ring and pericondensed aromatic species with repetitive structural features. For demonstrative purposes, details are provided for the CID of molecular ions at masses 202 and 434. Insights into the role of the aliphatically substituted and bridged aromatics in the reaction network of PAH growth chemistry were obtained from spatially resolved measurements of the flame. The experimental results are consistent with a growth mechanism in which alkylated aromatics are oxidized to form pericondensed ring structures or react and recombine with other aromatics to form larger, potentially three-dimensional, aliphatically bridged multi-core aromatic hydrocarbons.

Introduction

The chemistry of soot formation remains an intriguing problem in physical chemistry research. Over the years, a chemical description has been developed in which gas-phase precursor molecules react to form small aromatic species, which subsequently can undergo additional gas-phase reactions to form polycyclic aromatic hydrocarbons (PAHs).[1-3] While the transition from gas-phase PAHs to incipient soot particles is still not clear, it is expected that this nucleation step is followed by surface reactions and coagulation to allow for growth of the particles.

Because of the importance of the formation of the so-called "first aromatic" ring for the overall soot formation process, much experimental and theoretical research was focused on the formation of benzene, the simplest aromatic species.[4-6] For many flame configurations, it is now understood that benzene is formed through reactions of resonantly stabilized radicals such as C_3H_3 (propargyl), C_3H_5 (allyl), *i*-C_4H_5, and C_5H_5 (cyclopentadienyl).[7] The importance of the individual reactions can vary with the chemical structure of the fuel.[8-9] Furthermore, evidence in the literature suggests that other aromatic species, beyond benzene, can serve as the "first aromatic" ring. Notable examples are the formation of benzyl and naphthalene through reactions of cyclopentadienyl with C_2H_2 and another C_5H_5 radical, respectively.[10-11] Also, the C_5H_7 species can be interpreted as methyl-substituted *i*-C_4H_5 radicals as identified in flames and it has been proposed that they can form toluene in a reaction similar to *i*-C_4H_5+C_2H_2.[12]

While the formation of the "first aromatic" ring can be considered well understood at this point, the growth reactions to form polycyclic aromatic hydrocarbons (PAHs) and the reactions of their respective radicals are not entirely clear. The reasons for this can be found in the complexity of the PAH formation chemistry, *i.e.* the molecular size of the reactants, intermediates, and products provides a challenge for theoretical and experimental studies. As a consequence, the

identity of the intermediates has not been entirely resolved and missing validation targets in combination with missing kinetic parameters preclude the assembly of an accurate detailed model for PAH formation chemistry. In current mechanisms, the PAH formation is dominated by the so-called "Hydrogen-Abstraction-C_2H_2-Addition" (HACA) reaction sequence,[1-2, 13-14] but recent experimental and theoretical provide evidence for other potential PAH formation routes that should be explored. While the HACA sequence provided the framework for kinetic models describing PAH growth, it may not be generally valid for all conditions under which soot formation occurs.[15-23] While the investigation of the formation of the "first aromatic" ring has benefited greatly from kinetic calculations and modeling in combination with isomer-specific and spatially resolved measurements in flames,[4, 24-25] such an approach is currently not suitable for exploring PAH chemistry given the large number of different conceivable isomeric structures.[24]

Nevertheless, many different isomeric PAH structures have been identified experimentally in flame and pyrolysis experiments using a variety of different diagnostic techniques.[26] For example, flame-sampling mass spectrometry,[24-25, 27-29] aerosol mass spectrometry,[30-34] and gas-chromatography[35-37] have enabled the detection of molecules beyond the so-called "stabilomer grid".[38] Furthermore, infrared and mass spectra of extracted soot particles revealed the presence of saturated and unsaturated aliphatic hydrocarbon chains and of several oxygen-related functionalities.[39-42] Recently, x-ray based photoelectron spectroscopy has been used to identify oxygenated furan-like structures in sampled soot particles.[33] The exact identity and role of these functionalities in PAH and soot formation chemistry is currently not understood.

Because evidence is accumulating in the literature that suggests that pyrene dimerization is not a viable nucleation route,[43-44] alternative soot inception pathways are currently discussed, which, for example, include aliphatically substituted and aliphatically bridged polycyclic aromatic

hydrocarbons.[45-49] These classes of molecules are of interest because their complexes appear to be more stable than the pyrene dimers or they can occur in stable three-dimensional π-stack conformations.[3, 44-51] In this paper, we provide novel detailed experimental evidence for the presence and chemical identity of aliphatically substituted and aliphatically bridged multi-core PAHs as they occur in sooting flames. Instead of addressing the complexity of the PAH formation chemistry through isomer-specific measurements, we provide new insights towards a complete understanding of PAH and soot formation chemistry through the identification of aromatic structures and their aliphatic and aromatic hydrocarbon side chains. The results, which are made possible by employing an advanced diagnostics tool based on the principle of tandem mass spectrometry,[52-53] are consistent with a chemical mechanism of PAH growth in which aliphatically substituted and bridged PAHs are of importance.

Experimental Details

Experiments were performed using a laboratory-scale ethylene/O_2 coflow diffusion flame at atmospheric pressure that was stabilized on a stainless-steel burner. This configuration ensured the stability of the flame over a wide range of conditions that were tested for optimization of the sampling process and ionization scheme while forming sufficient amounts of PAHs in spatially resolvable parts of the flame. The burner consists of three concentric stainless steel tubes with inner diameters of 14, 20 and 50 mm, respectively. In the inverse configuration used here, the O_2 stream of 240 sccm was metered through the inner concentric tube together with a dilution of 960 sccm N_2. The ethylene flow of 310 sccm through the second concentric ring was diluted with 1000 sccm of N_2. The flame was surrounded by an N_2 sheath flow of 20 slm. The entire burner assembly has been mounted on a motor-controlled x-y translational stage to allow for probing

various positions in the flame with an accuracy of ±0.05 mm. The burner was housed in a fixed chimney with bellows sealing around the gap between the stage and the chimney. The two-dimensional temperature profile of the flame was measured using an R-type thermocouple and the results are provided in Fig. S1 of the Supplementary Material.

The experimental set-up used to unravel the core structural features in the PAH formation reaction network in combustion environments is shown schematically in Fig. 1. The gaseous components of the flame are sampled at atmospheric pressure through a 0.5 mm diameter pinhole in a stainless-steel tube. The sampled gases are immediately diluted with N_2 at the sampling point to avoid nucleation and condensation during the sampling process and ion-molecule reactions in the ionization region. A ratio of sampled gas to dilution of 1:150 was found optimal and allowed also for the detection of radical species as described below.

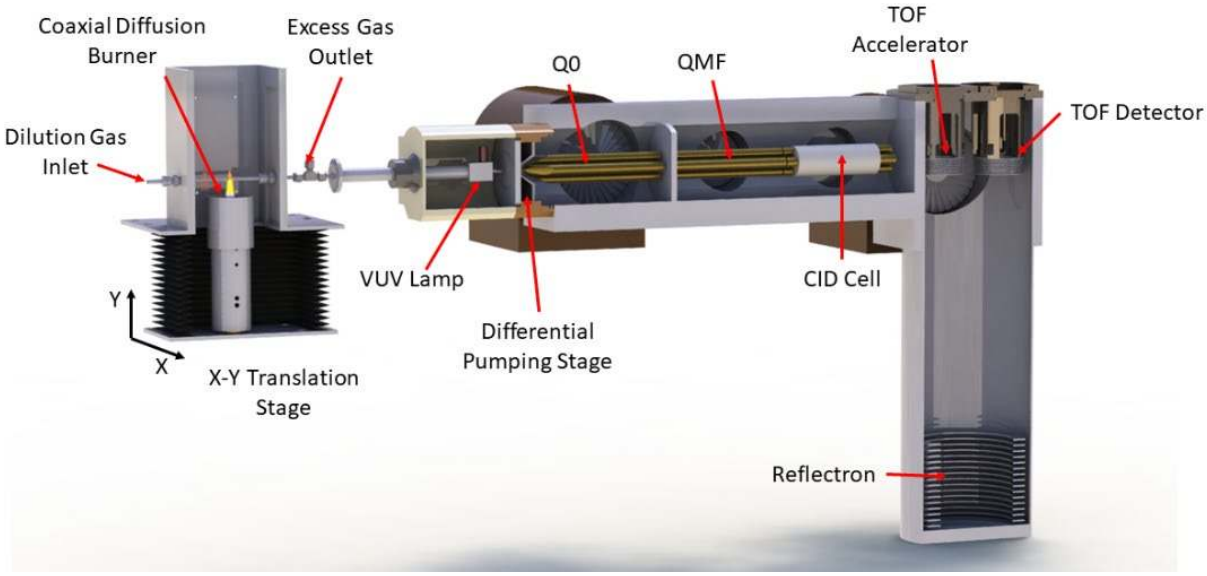

Figure 1: Rendering of experimental setup. See text for details.

The sampled and dilution gases are delivered to the inlet of a modified AB Sciex *QSTAR Elite* APPI-Q-CID-TOF mass spectrometer. The atmospheric pressure photoionization (APPI) source for this mass spectrometer would ordinarily include a heated nebulizer (to aerosolize and evaporate liquid samples, prior to irradiation with light from a 10.0 eV krypton VUV lamp), but this has been removed and replaced with a 6.35 mm O.D. stainless steel tube, through which sampled gases are delivered to the VUV lamp. From this point, the instrument is consistent with a standard QSTAR Elite.

Flame-sampled species are ionized in a single-photon ionization process using the 10.0 eV photons from the VUV lamp. This energy is sufficient to ionize the aromatic species in the mass range of up to 1000 Da this paper is focusing on while ensuring near-threshold ionization, thus minimizing dissociative photoionization processes.[34] Given the high density of gases in the APPI source, the sensitivity of this instrument is expected to be significantly higher than conventional flame-sampling mass spectrometers, in which ionization traditionally occurs after the formation of the molecular beam.[24-25] As shown below, this setup allows for the detection of high-mass radical species.

Following passage through the VUV lamp, the ions pass through two stages of differential pumping. The first is pumped by a mechanical pump, and consists of a short gap between the inlet orifice and a skimmer. A ring electrode between the inlet orifice and the skimmer focuses ions through the skimmer. Potentials are also applied to both the inlet plate and the skimmer in order to accelerate the ions, causing collisions with neutral gas molecules resulting in declustering. A quadrupole ion guide (Q0) steers the ions through the second differential pumping region, which is evacuated by a 700 L/s turbomolecular drag pump (Leybold TW700) achieving a pressure of approximately 10 mTorr. Collisions between ions and the relatively high pressure of neutral gas

in this chamber dampen oscillatory motion of the ions in Q0 resulting in a more focused beam of ions.

Following Q0, the ions pass through an aperture into a chamber that contains the quadruple mass filter (QMF) and collision induced dissociation (CID) cell. The QMF is operated in either an ion guide mode or a mass-selective mode, depending on whether an overall or MS-MS spectrum is to be collected. The first mode is referred to as "TOF" mode, whereas the second mode of operation is referred to as "MS-MS" mode. The CID cell contains a linear quadrupole ion trap, in which ions are fragmented through collisions with neutral gas molecules (argon). The extent of fragmentation is primarily determined by the initial velocity of the ions, which is a function of the difference between the DC bias applied to Q0 and the bias applied to the CID cell. If no fragmentation of ions is required, then the CID cell is simply used to accumulate ions; no gas is fed to the CID cell, and the difference in DC bias is kept small. Examples will be discussed below, in which the automated scanning of the collision energy, *i.e.* of the velocity of the ions, in both the TOF and MS-MS mode was used to extract structural information of the sampled flame components. Although the structural rearrangements and fragmentations occur on the ion potential energy surface, the tandem mass spectra allow for extraction of structural information of the neutral, but the interpretation of the MS-MS spectra might be complex.

Parent and fragment ions are periodically pulsed out of the CID cell. A repetition rate of 7 kHz was applied to allow for covering the targeted mass range of up to 1000 Da. The ions pass through an aperture into the time-of-flight (TOF) chamber, in which the ions are separated by their flight time towards a micro-channel plate detector. To achieve a FWHM mass resolution of ~8000, a reflectron is used for energy focusing. Mass spectra are typically accumulated for about one

second at any point in the given parameter space, *e.g.* collision energy scans, two-dimensional burner-position scans.

Results and Discussion

(a) Overview Mass Spectra and Identification of Foundational PAH Structures:

Before the spectra obtained in the mass specific tandem MS-MS spectra are discussed in more detail, it is essential to describe the overall flame-sampled CID mass spectra in the TOF mode. Figure 2 shows overview mass spectra from two different sampling points obtained in the TOF mode, taken at low (1-5 eV) CID collision energies where fragmentation was mainly avoided. As described above, the overview mass spectra, which cover the mass-to-charge range of m/z = 0-800 Da, were taken at sufficient dilution to minimize nucleation and ion-molecule reactions.

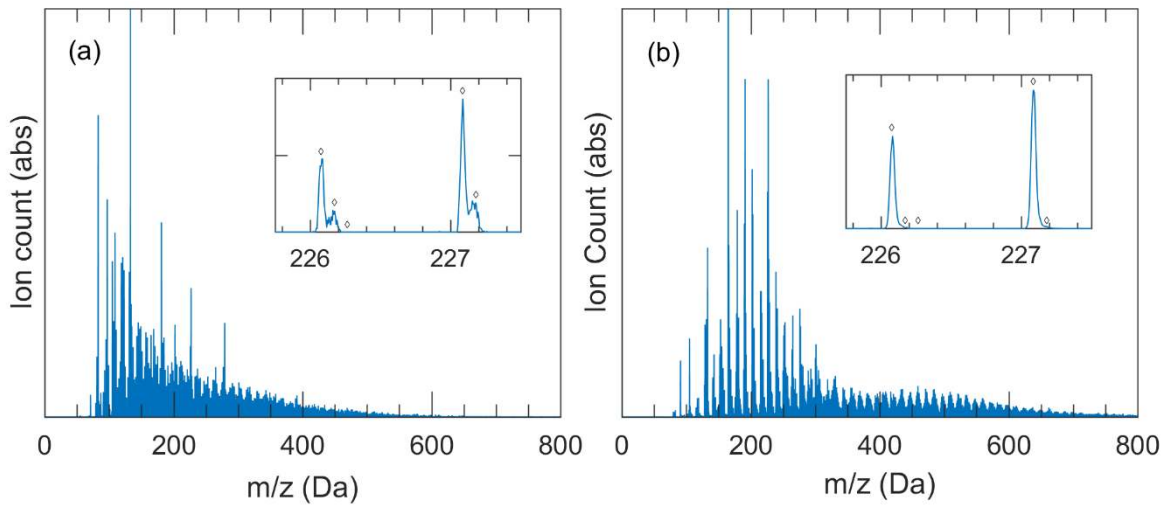

Figure 2: Averaged mass spectra at low (1-5 eV) CID collision energies, sampled from different flame regions. (a) Short distance above the fuel outlet in the fuel pyrolysis zone. (b) On the centerline above the flame. The inserts show zoomed-in regions of the mass spectra covering the range near 226 and 227 Da. Exact masses for (a) $C_{18}H_{10}$, $C_{17}H_{22}$, and $C_{16}H_{34}$ and (b) $C_{18}H_{11}$ and $C_{17}H_{23}$ are indicated by the dots. See text for details.

The recorded mass spectra appear to be similar to flame-sampled mass spectra reported in the literature,[54-57] although the relative intensity of the different peaks should be interpreted with caution given the transmission curves of the QMF for different mass ranges. The sampled mass spectra reveal the complexity of the chemical reaction network of the combustion processes and highlight the difficulty of accurate isomer-specific measurements. These facts become even more visible when zooming in on individual mass-to-charge ratios. As shown in the inserts in Fig. 2(a) and (b), the resolution of the reflectron time-of-flight mass spectrometer allows for the detection of different species with the same nominal mass. In Fig. 2(a), for the nominal masses *m/z* of 226 and 227, two different peaks are clearly visible on each mass unit that correspond to $C_{18}H_{10}$ (*m/z* = 226.078), $C_{17}H_{22}$ (*m/z* = 226.172), and $C_{18}H_{11}$ and $C_{17}H_{23}$, (*m/z* = 227.086 and 227.180), respectively. $C_{18}H_{10}$ intermediates are typically assumed to be pericondensed ring-structures as they have been identified in respective gas-chromatography experiments.[41-42] However, many other isomeric structures are conceivable. The presence of the $C_{17}H_{22}$ and $C_{17}H_{23}$ intermediates points towards the presence of alkylated aromatic species.

In general, different species appeared at each nominal mass, corresponding to aromatic species with chemical compositions of C_xH_y, and $C_{x-1}H_{y+12}$; in addition, single- ($C_{x-1}H_{y-4}O$ and $C_{x-2}H_{y+8}O$) and double- ($C_{x-3}H_{y+4}O_2$) oxygenated aromatic species were detected as well. In previous measurements using flame-sampling mass spectrometry or aerosol mass spectrometry,[9, 31-34, 54-58] the resolution of the mass spectrometers has not been sufficient to reveal the complexity of this PAH formation chemistry with this level of detail. However, the results here are consistent with the detection of aliphatic and oxygenated components absorbed on sampled soot particles.[39-42, 48] This complexity of the mass spectra has precluded a detailed correction of the ^{13}C and ^{18}O

isotopomeric contributions to individual mass peaks and, for the *m/z* = 202 and 434 discussed here specifically, it was verified that this simplification does not change the conclusions.

The aromatic character of the sampled gaseous species was confirmed by the fragmentation mass spectra taken in the TOF mode. To this end, the evolution of the flame-sampled mass spectra was recorded as a function of the collision energy in the CID cell. Results are shown in Fig. 3 for the two different sampling positions identified in Fig.2, which exhibit large amounts of the C_xH_y, and $C_{x-1}H_{y+12}$ intermediates. For easy comparison, Fig. 2(a) has been included in Fig. 3 as panel (a). A visual comparison of panels (a) and (b), representing accumulated fragmentation mass spectra applying 1-5 eV and 20-30 eV collisional energy, respectively, shows that at intermediate collision energies, the ions in the mass range above ~300 Da fragment first. Although, it is also seen that the mass spectral range below is starting to be less crowded compared to the low CID collision energy mass spectrum. At these intermediate collision energies, the mass spectrum contains signal from intact parent ions along with fragment ions from larger species. This fragmentation mass spectrum indicates that the heavier intermediates are more weakly bound than the lighter molecules and that the latter are building blocks of the heavier intermediates. This statement is an interpretation of the tandem mass spectra based on knowledge from fragmentation mechanisms of pericondensed aromatic rings with no side chains that are unlikely to fragment at low and intermediate collision energies.[59-62] Similar experimental results do not exist for the aliphatically substituted and bridged structures discussed here, but using bond dissociation energies of various model compounds, it will be discussed further below, that the observations from Fig. 3 point towards the presence of aliphatically bridged multi-core aromatic species.

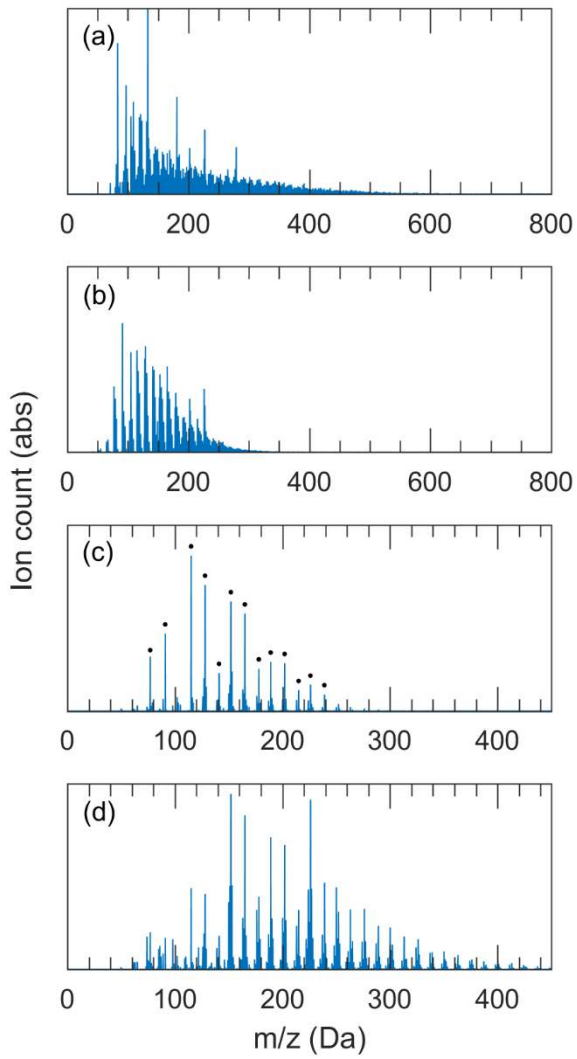

Figure 3: Averaged mass spectra at (a) low (1-5 eV), (b) intermediate (20-30 eV), and (c) high (90-100 eV) CID collision energies. Sampling position was identical to Fig. 2(a). (d) High (90-100 eV) CID collision energy mass spectra after sampling in the aromatics region identical to Fig. 2(b). See text for details. Different mass ranges are shown for panels (a) and (b) than for (c) and (d).

For even higher collision energies, *i.e.* 90-100 eV [panel (c); please note the different scales on the x-axis between panels (b) and (c)], only certain peaks appear in the fragmentation mass spectra. These marked peaks include (with likely molecular structures provided in parenthesis): *m/z* = 77.039 (C_6H_5, phenyl), 91.055 (C_7H_7, benzyl), 115.055 (C_9H_7, indenyl), 128.063 ($C_{10}H_8$, naphthalene), 141.070 ($C_{11}H_9$, methylnaphthyl radical), 152.063 ($C_{12}H_8$, acenaphthylene and/or ethynylnaphthalene), 165.070 ($C_{13}H_9$, fluorenyl and/or phenalene radicals), 178.078 ($C_{14}H_{10}$,

anthracene and/or phenanthrene), 189.070 ($C_{15}H_9$, 5H-benz[fg]acenaphthylene and/or 4H-cyclopenta[def]phenanthrene radicals), 202.078 ($C_{16}H_{10}$, pyrene and/or fluoranthene), etc.

When sampling in the same region of the flame as for Fig. 2(b), in which intermediates of up to 800 Da are detectable, the list of foundational aromatic structures in the fragmentation mass spectra extends beyond *m/z* = 400 Da as seen in Fig. 3(d). Furthermore, a comparison between Figs 3(c) and (d) also reveals a shift in intensities towards heavier masses and the peaks at *m/z* = 152.063 ($C_{12}H_8$) and 226.078 ($C_{18}H_{10}$) have become the most prominent peaks in the fragmentation spectrum. Although these tandem mass spectra do not provide direct information about the PAH growth chemistry processes, they reveal the structures of the aromatic buildings blocks of the sampled gaseous intermediates that play an important role in the PAH growth chemistry.

The list of the foundational PAH structures shown in Fig. 3(c) and (d) is best described as a network of closed-shell and radical species as shown in Fig. 4. In this Figure, benzyl and phenyl radicals are the starting blocks of PAH formation and the rest of the foundational PAHs observed in this experiment are explainable by enlarging the seed molecule through addition of peri-condensed rings (vertical axis) or through addition of C_2 units (horizontal axis). Only the most intense peaks are highlighted graphically in Fig. 4, and this network expands beyond the listed species. Radical species (with the exception of phenyl) are highlighted in blue and contain an odd number of carbon atoms. These species may possibly contain five-membered ring-structures. While this graph does not make an assumption of the chemical pathways, it is consistent with the current understanding of PAH formation through various channels, including methyl- and phenyl-radical addition,[23, 63] cyclopentadienyl reactions (including ring-enlargements),[10-11] HACA steps,[14, 22, 58] etc. Molecular growth represented along the horizontal lines is best explained through HACA-like steps in which a C_2H_2 unit bridges the C-C-C-C boat configuration as exemplified in

phenanthrene (forming pyrene), or the C-C-C zigzag configuration in naphthalene (forming a five-membered ring structure like acenaphthylene).[15, 64] To clarify the importance of the different reaction pathways that could connect the observed foundational PAH building blocks, chemical kinetics modeling is needed, a task that is beyond the scope of the present work.

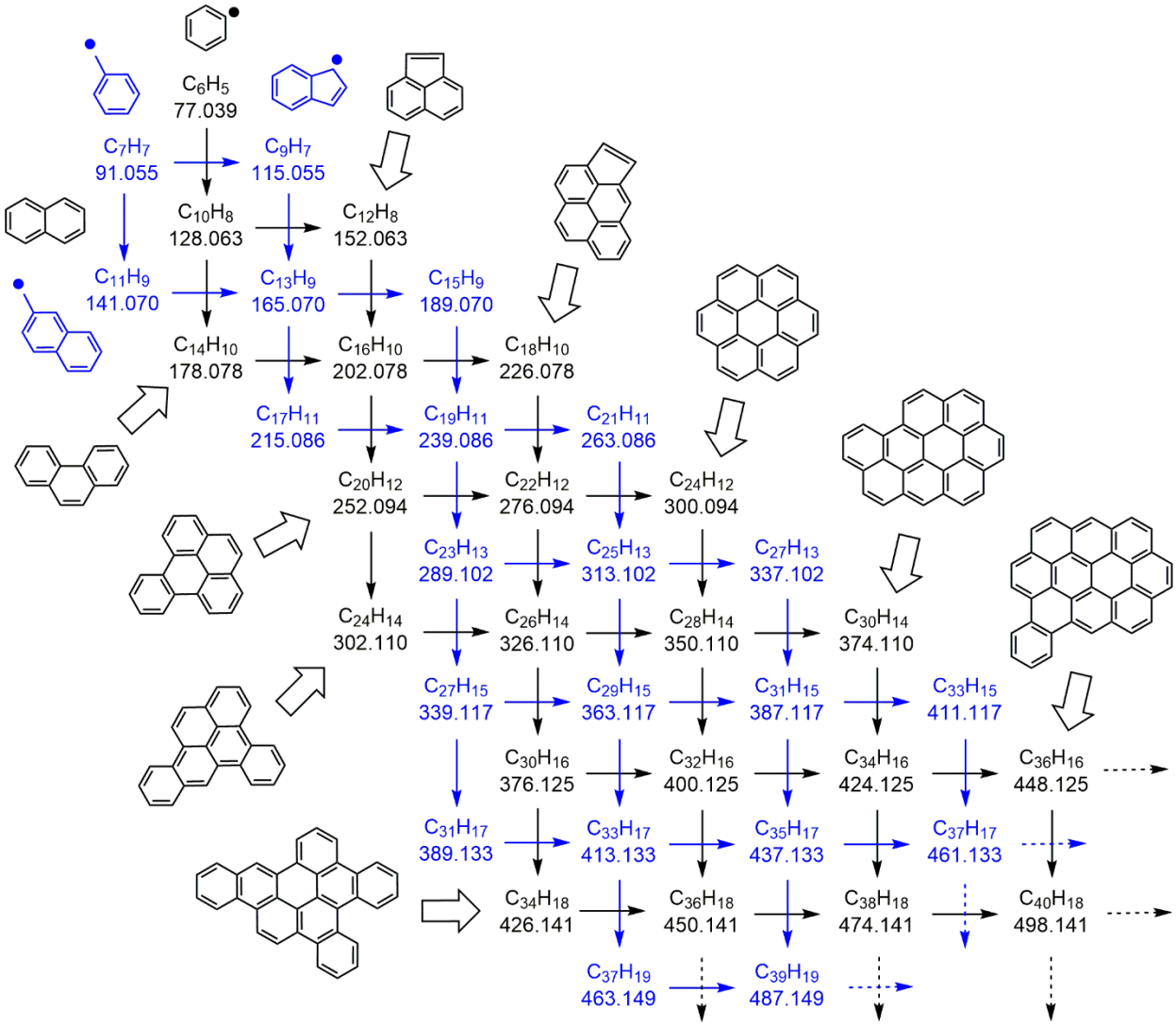

Figure 4: Graphical visualization of the experimentally observed foundational PAHs. The observed tandem mass spectra can be explained by a network of intermediates that is characterized through addition of peri-condensed aromatic rings and C_2 units.

The fragmentation scans reveal the need to differentiate between four different classes of aromatic hydrocarbon compounds (note that we will not consider the oxygenated species in this paper). For C_xH_y with a C/H ratio of ≥ 1, the first three classes are (a) pericondensed aromatic ring structures like pyrene and fluoranthene ($C_{16}H_{10}$) and biphenyl-like structures, (b) pericondensed ring structures with a single short side-chain like -CH_3 or -C_2H (for example, $C_{17}H_{12}$ or $C_{18}H_{10}$) or five-membered ring structures with a bridged C-C-C zig-zag feature like in acenaphthalene, and (c) aliphatically bridged multi-core aromatics. For $C_{x-1}H_{y+12}$ with a C/H ratio of < 1, the fourth class is (d) aliphatically substituted (or alkylated) aromatic rings, *i.e.* aromatics with multiple side-chains like $C_{17}H_{22}$.

While plenty of evidence is already provided in the literature for the presence of aromatic species of types (a), (b), and (d) in combustion environments,[35, 41-42, 65-69] this paper discusses the identification of the structural features of the alkylated [type (d)] at an unprecedented level of detail. Furthermore, this paper describes the detection of aliphatically bridged multi-core aromatic ring structures [type (c)], which so far have only been hypothesized to be present in flames.[45-46, 70] Chemical structures of these previously elusive intermediates are proposed.

Evidence for the presence of the aliphatically substituted (or alkylated) aromatic ring structures [like $C_{17}H_{22}$ (m/z = 226.172) and $C_{17}H_{23}$, (m/z = 227.180)] were already presented in the flame-sampled high-resolution mass spectra as shown in Fig. 2(a). While the fragmentation time-of-flight mass spectra provide evidence for the aliphatically bridged intermediates, additionally it is shown that these previously unidentified intermediates can be distinguished from the other C_xH_y aromatics based on the mass-specific fragmentation mass spectra.

(b) Spatially Resolved Mass Spectra:

Having detected the two groups of aromatic compounds (C_xH_y and $C_{x-1}H_{y+12}$), spatially resolved measurements become necessary to visualize their respective position in the flame and to eventually gain insights into the role of the different classes of aromatics in PAH formation chemistry. To this end, mass spectra in the TOF mode and collision energies of 5 eV were recorded in pre-programmed two-dimensional scans along the x- (horizontal) and y- (vertical) axis. A stepsize of 0.5 mm was chosen in the horizontal direction to cover a range from -5 to 20 mm (with the origin over the center of the O_2 outlet). A range from 4 to 32 mm was covered in the vertical direction in steps of 1.0 mm. The results are shown in Fig. 5, which shows the two-dimensional color maps of the sum of ion counts of all detected masses in the range from 200 to 300 Da. In this two-dimensional figure, the even (closed shell molecules) and odd masses (radicals) and aromatic species with C/H ratio > 1 (labeled Aromatics) and aromatics with C/H ratio < 1 (labeled Alkyl – for the alkyl side-chains) are shown separately. The sum of ion counts is shown as different colors and represent the aggregates of all ions within one peak halfwidth of the exact masses of each ion type.

Each color map is scaled individually, and a visual comparison reveals that the signal of the closed shell molecules is dominated by the aromatic compounds formed in the pyrolytic zone of the flame, while radicals are more likely to be detected in the form of the alkylated aromatics. The spatial separation of odd and even masses indicates that the radicals are not formed from dissociative ionization or other reactions in the ionization region. The fact that odd masses are detectable independent of the even masses indicates that the immediate dilution at the sampling position significantly inhibits further reactions of the sampled gas-phase species, thus ensuring that the mass spectra accurately replicate the gaseous composition at the sampling position. The

region of odd aromatics beyond 10 mm on the radial axis includes ^{13}C contributions of the even masses, for which no correction has been made.

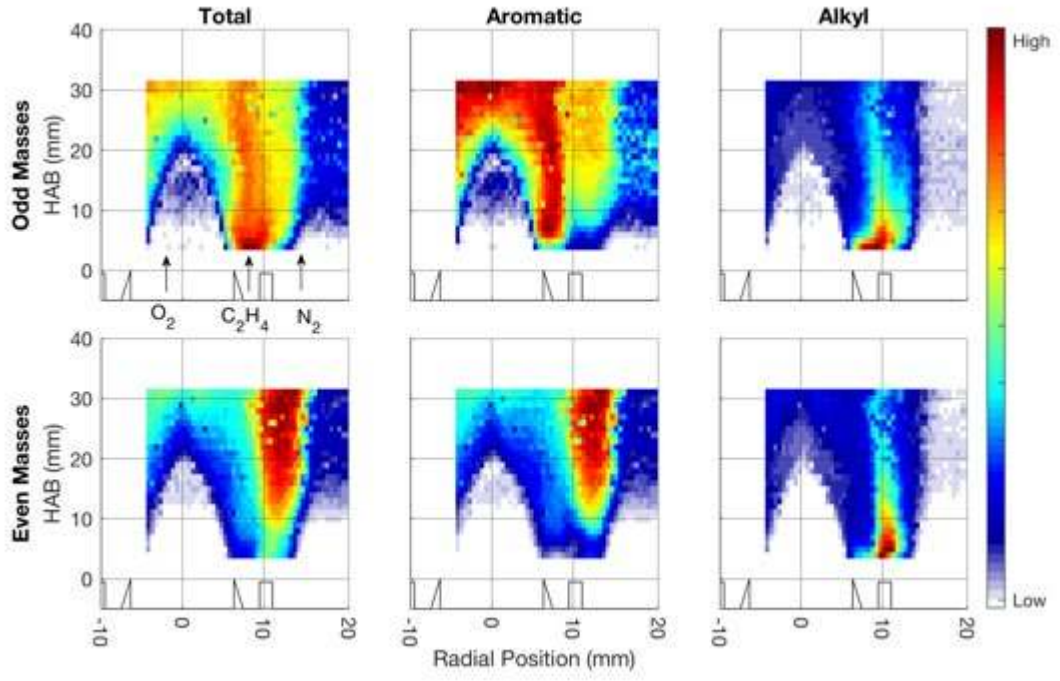

Figure 5: Two-dimensional color maps of ion counts across the ethylene/O_2 inverse co-flow flame shown in a linear scale (blue: low ion counts; red: high ion counts). Left column: total ion count; middle column: aromatic hydrocarbons with C/H > 1; right column: alkyl-substituted aromatics with C:H < 1. The upper row includes odd masses (radical species), the bottom row includes even masses. The cross (position #1) and circle (position #2) in the upper left heatmap indicate the two different sampling positions for the data discussed here in detail.

Besides the spatial separation of the odd and even masses, Fig. 5 reveals the spatial separation of aromatic species with C/H > 1 from the alkylated aromatics with C/H < 1. In the mass range from 200-300 Da, the formation of aromatic species of the types (a)-(c) appears to follow the formation of the alkylated aromatics. This observation is consistent with a mechanism in which small precursor molecules form small aromatic rings, most likely benzene, which then subsequently grow to form alkylated aromatics in the mass range of 200-300 Da. These

components then get oxidized to form condensed aromatic rings with fewer (and probably more unsaturated side-chains) and potentially aliphatically bridged aromatics (see below). While detailed mechanistic insights cannot be gained from the mass spectra, it is expected that in the oxygen-rich zone of the flame, the oxidation steps proceed through H-abstraction reactions by O_2 or by the abundant O, OH, and HO_2 radicals. At the high-temperatures of the flame, the PAH radicals can further dissociate via β-scission reactions, isomerize, or recombine.

At higher masses, *i.e.* 600-700 Da, the condensed aromatic rings appear to be more intense than the aliphatically substituted aromatics for both odd and even masses. The intensity maps for these two classes of aromatics are shown in Fig. S2 of the Supplementary Material. In this larger mass range, aliphatically substituted aromatics overlap spatially with the other aromatic structures, thus indicating that in this mass range, the oxidation of the aliphatically bridged aromatics is not the only important formation pathway. Other potential formation pathways that co-exist include, for example, the radical-radical recombination reactions.

(c) Structural Features Identified by Tandem MS-MS:

In this Section, the mass-selected tandem MS-MS spectra are discussed as they were found to be instrumental to identify the structural features of the flame-sampled PAH molecules. While it is beyond our means to provide detailed information from this very rich multi-dimensional (x, y, mass, collision energy) data space, we will only describe a few characteristic fragmentation MS-MS spectra to showcase the potential of tandem mass spectrometry and to discuss reoccurring structural features. The following discussion will focus on *m/z* = 202 ($C_{16}H_{10}$ and $C_{15}H_{22}$) and 434 ($C_{34}H_{26}$ and $C_{33}H_{38}$), where detailed identification will be provided for aliphatically substituted

and bridged aromatic species. ^{13}C isotopic contributions from the respective *m/z* = 201 and 433 signals were neglected as the respective signal intensities were significantly smaller than the *m/z* = 202 and 434 signals.

The structural features of the aliphatically substituted aromatics are unraveled using the above described MS-MS mode of the mass spectrometer. Figure 6 shows the results of the fragmentation MS-MS spectra for *m/z* = 202 after sampling at position #1 and #2 (see Fig. 5 for the respective sampling position). In these plots, the intensity of the peaks is shown as functions of the *m/z* ratio of the parent and fragment ions (x-axis) and the collision energy (y-axis).

The top panel shows the fragmentation pattern of the pure $C_{16}H_{10}$ sampled from the aromatic hydrocarbon (position #2, see Fig. 5) as can be seen in the insert that shows that mass spectra of the parent peak. The bottom panel shows the fragmentation mass spectra at sampling position #1 (see Fig. 5) that contains both, the pericondensed $C_{16}H_{10}$ and the aliphatically substituted $C_{15}H_{22}$ aromatics.

The absence of fragments at low collision energy in the top panel reveals the stability of the $C_{16}H_{10}$ isomers. Upon collision with Ar atoms in the collision cell, the isomers tend to consecutively lose H-atoms leading to fragment ions at *m/z* = 201 – 198. The carbon atom framework stays intact until collision energies of 35 to 40 eV. The corresponding fragment peaks at *m/z* = 174.047 and 176.063 indicate the loss of two C-atoms (plus four and two H-atoms, respectively) from the stable PAH structure, while the formation of *m/z* = 150.047 and 152.063 fragments originate from the loss of 4 C-atoms (plus four and two H-atoms, respectively). This dissociation behavior is consistent with pericondensed aromatic ring structures and expected for species like pyrene and fluoranthene.[60-61, 71-72] Because the dissociation channels are similar for these PAHs, no isomeric information can be gained from these MS-MS data. At high enough

collision energies, *i.e.* above 60 eV, the formation of polyynic structures (C_8H_2 and $C_{10}H_2$ at *m/z* = 98.016 and 122.016, respectively) is observed, also a known feature of PAH ion dissociation chemistry.[73]

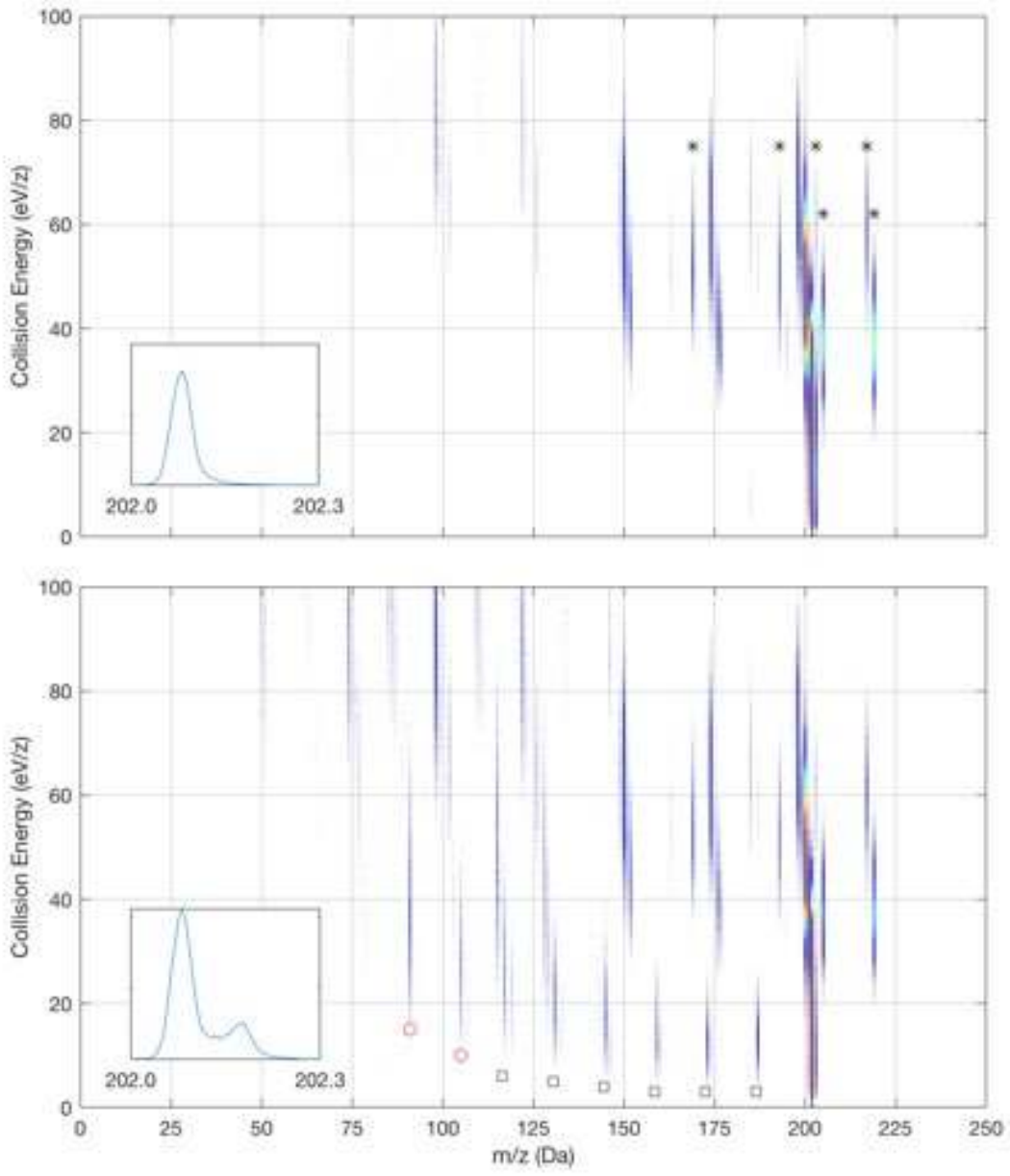

Figure 6: Fragmentation MS-MS spectra of *m/z* = 202 at two different sampling positions. Top: Only $C_{16}H_{10}$ isomers are present as parent ion, as sampled at position #2 (see Fig. 5). Bottom: Both $C_{16}H_{10}$ and $C_{15}H_{22}$ are present, as sampled at position #1 (see Fig. 5). Fragment ions after loss of alkyl-side chains are marked with squares in the bottom panel. The foundational aromatic structures (*m/z* = 91 and 105) are marked with circles.

Observed mass spectral signals marked with an asterisk in the upper panel of Fig. 6 result from water-ion clustering in the collision cell due to some water background. Because of their specific *m/z* ratio and the oxygen content, these mass spectral peaks are easy to identify in the analysis and do not need to be further considered.

The differences in the fragmentation MS-MS spectra of Fig. 6 become immediately visible when the parent ion contains $C_{15}H_{22}$ in addition to the $C_{16}H_{10}$ compounds. As can be seen in the bottom panel of Fig. 6, the features from 150 to 200 Da at high collision energies are identical to those discussed above and likely belong to the $C_{16}H_{10}$ isomers. However, additional features are seen, among which are the loss of alkyl groups at relatively low collision energy. The corresponding peaks are marked (with squares) and correlate to loss of mass units that are identical to saturated alkyl chains, *i.e.* loss of CH_3, C_2H_5, C_3H_7, C_4H_9, C_5H_{11}, and C_6H_{13}. Under these conditions, there is no evidence for the loss of unsaturated side-chains or the presence of the unsaturated side-chains in the observed molecular structures. Instead, the core aromatic structures of the $C_{15}H_{22}$ isomers (marked with circles) were identified as benzyl (C_7H_7) at *m/z* = 91.055 and xylyl (C_8H_9) at *m/z* = 105.070. The features at *m/z* = 116.063 and 128.063 (indene and naphthalene) are probably fragments (-H) from the fragments at 119.086 and 130.078, respectively.

In this specific case of $C_{15}H_{22}$, it is assumed that the isomeric structures consist of one-ring aromatics with multiple aliphatic side-chains and/or a condensed aromatic-saturated ring structure. Some examples of possible $C_{15}H_{22}$ structures are shown in Fig. 7. While this Figure is certainly not a complete representation of detected $C_{15}H_{22}$ isomers, it highlights the structural differences that can occur including number of aliphatic side-chains, their length, and their linear *vs.* branched character.

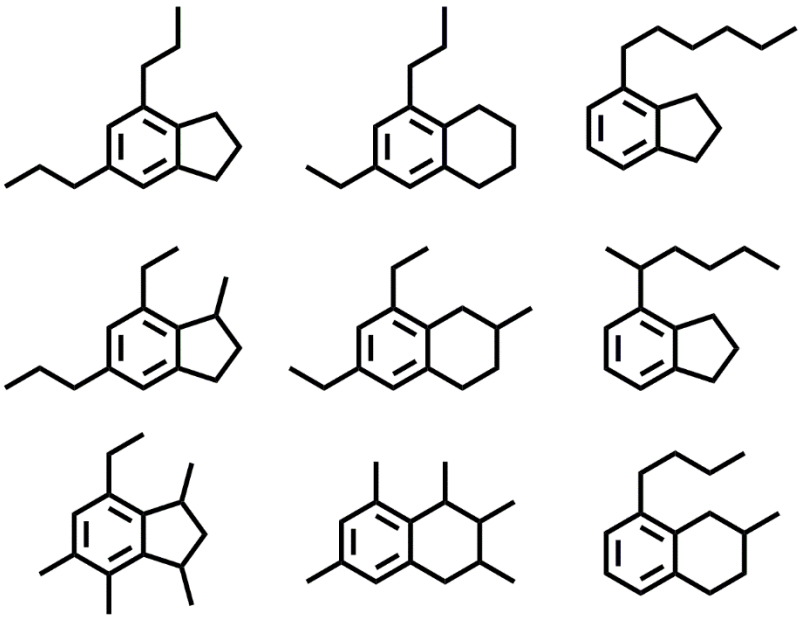

Figure 7: Conceivable $C_{15}H_{22}$ isomers, based on the detection of aliphatic side-chains and foundational aromatic structures in the flame-sampled tandem mass spectrum. Many more different isomers are conceivable and this short list only highlights the diversity of different structural features.

The observation of saturated alkyl groups is consistent with earlier work, in which such functional groups were observed, although not directly in the gas phase, using infrared spectroscopy on sampled nascent soot particles.[39-40] Furthermore, the observed presence of saturated alkyl groups is also in agreement with earlier work that pointed out the importance of reactions of methyl radicals for the PAH formation chemistry.[58, 63]

Alkylated side-chains are detectable throughout the flame-sampled mass spectra. As an additional example, we discuss here the fragmentation MS-MS of $m/z = 434$. The results are shown in Fig. 8. The overview mass spectra as function of the collision energy are plotted in Fig. 8(a) and the rich MS-MS spectra show the intricacy of the chemical structures of the flame-sampled PAHs. The mass spectrum at the parent mass is shown in the insert, with the accurate masses marked for

the pure hydrocarbons that correspond to $C_{36}H_2$ (*m/z* = 434.016), $C_{35}H_{14}$ (*m/z* = 434,110), $C_{34}H_{26}$ (*m/z* = 434.203), $C_{33}H_{38}$ (*m/z* = 434.297), $C_{32}H_{50}$ (*m/z* = 434.391), and $C_{31}H_{62}$ (*m/z* = 434.485). As can be seen, the observed signal corresponds mainly to $C_{33}H_{38}$, with smaller and minor contributions from $C_{34}H_{26}$ and $C_{32}H_{50}$.

While a detailed interpretation of the MS-MS spectra as shown in Figs. 6 and 8(a) is challenging, some important features are visible that allow for the extraction of important structural information of the sampled flame species. For example, as for *m/z* = 202, the losses of alkylated side-chains are observable in the MS-MS spectra of *m/z* = 434 as well. The corresponding loss of $-CH_3$, $-C_2H_5$, and $-C_3H_7$ are marked in Fig. 8(b), which shows the integrated mass spectrum covering a collision energy range from 1-15 eV. The high-resolution mass spectra revealed that these fragments arise from both the $C_{33}H_{38}$ and $C_{34}H_{26}$ parent ions. While the loss of heavier aliphatic fragments are also observable in the mass spectra, the strong intensity of the peaks in the same peak cluster seems to be shifted towards the loss of unsaturated side-chains, including $-C_4H_7$, $-C_5H_6$, $-C_6H_8$, etc. The loss of C_7H_7 (most likely benzyl), marked with a square, provides clear evidence for the presence of aliphatically bridged multi-core PAHs.

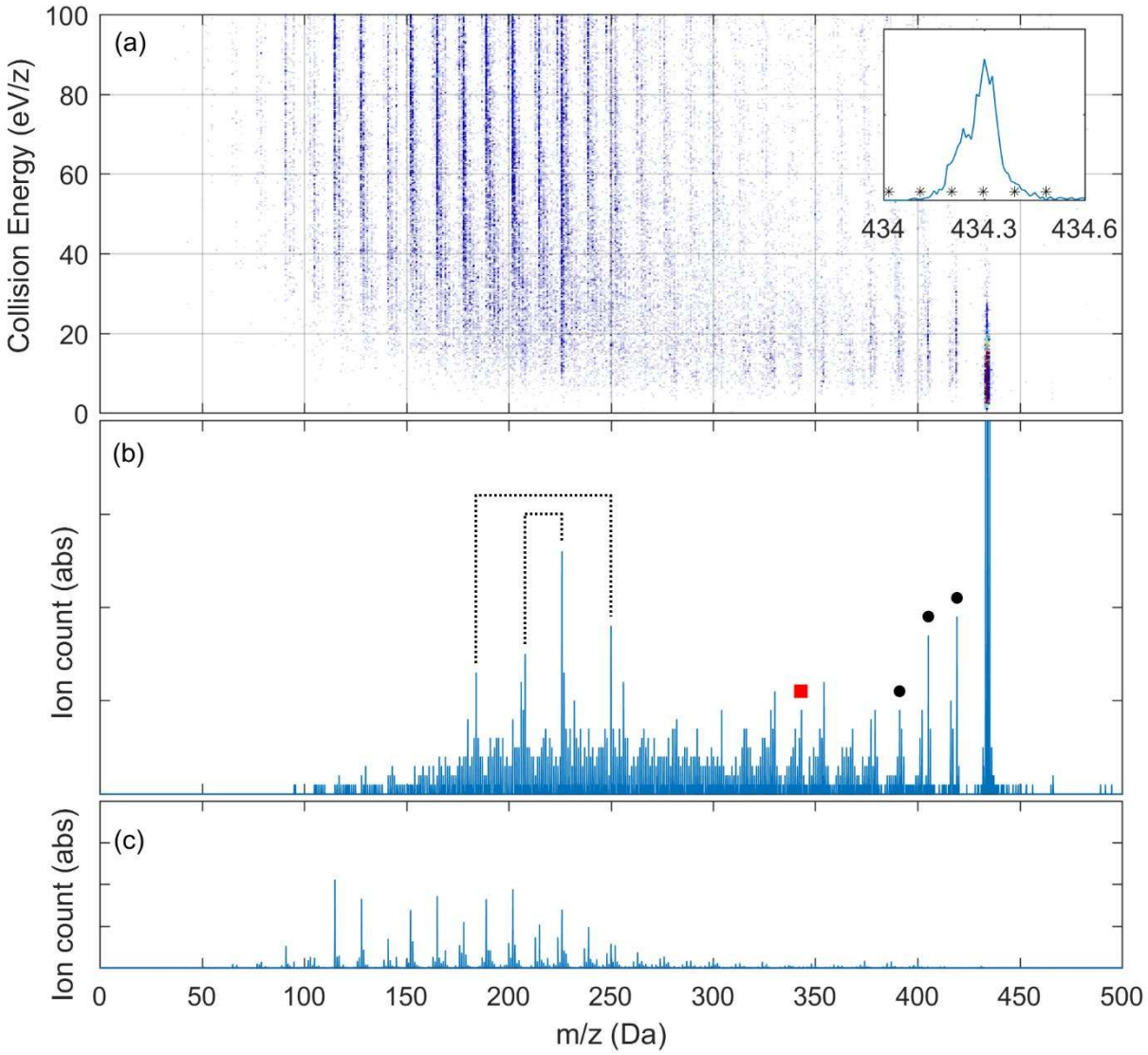

Figure 8: (a) Fragmentation MS-MS mass spectra of *m/z* = 434 as the function of collision energy. The inset shows the mass spectrum at the parent mass and reveals the presence of $C_{34}H_{26}$, $C_{33}H_{38}$, and $C_{32}H_{50}$ intermediates. (b) Integrated mass spectrum including collision energies from 1-15 eV. Some important features are marked; see text for details. (c) Integrated mass spectrum at high collision energies (90-100 eV) revealing the core PAH structures.

Further evidence in the MS-MS spectra for the multi-core PAHs is provided in the simultaneous detection of fragments and counter-fragments at relatively low collision energy. The identified molecules have enough rotatory degrees of freedom or are flexible enough to form three-

dimensional structures. Two pairs, *m/z* = 202.078 (+232.125) and 208.125 (+226.078), are indicated in Fig. 8(b). From the signal intensities of individual *m/z* ratios as function of the collision energy (shown for the ion pairs at 202.078+232.125 and 208.125+226.078 in Fig. 9), it can be concluded that the pairs consist of a stable fragment ($C_{16}H_{10}$ at *m/z* = 202.078 and $C_{18}H_{10}$ at *m/z* = 226.078) and a counter-fragment that through additional collisions dissociates further at larger collision energies and is thus characterized through a more aliphatic character ($C_{18}H_{16}$ and $C_{16}H_{16}$, respectively). Fig. 9 indicates that the stable ions are formed more readily and that the less stable fragment ions dissociate further at larger collision energies.

In summary, these pairs are best described through four characteristics: (a) they result from the parent ion with the larger C/H ratio, *i.e.* $C_{34}H_{26}$, (b) the fragments have similar masses and the charge can be on either of the fragments, (c) these fragments appear simultaneously at relatively low collision energies [see Fig. 8(a) and (b)], and (d) the pairs consist of a stable fragment and a counter-fragment that through additional collisions dissociates further at larger collision energies and is thus characterized through a more aliphatic character ($C_{18}H_{16}$ and $C_{16}H_{16}$, respectively).

Considering that the C-C bond dissociation energies of ethyl benzene ($C_6H_5CH_2$-CH_3) and bi-benzyl ($C_6H_5CH_2$-$CH_2C_6H_5$), are comparable (76.4 *vs.* 62.6 kcal/mol) and that the C-C bond in biphenyl (C_6H_5-C_6H_5) is much stronger, *i.e.* 111.4 kcal/mol,[74] these results indicate that the fragments were bound not through bi-phenyl type bonds that would be expected from aromatic radical-radical type reactions, but through aliphatic chains. Furthermore, these fragments appear at low collision energies also found for alkylated aromatics (see Fig. 6).

Figure 8(c) shows the integrated high-energy (90-100 eV) fragmentation MS-MS for *m/z* = 434. The same foundational PAH structures that were identified in Figure 3(c) and (d) for the entire flame-sampled mass spectra were detected here for a single mass unit. This fact is important.

On one hand, it can be interpreted as if the overall complexity of the PAH formation chemistry becomes visible already when interpreting contributions from a single mass. On the other hand, the similarity of the MS-MS spectra in Figs. 3 and 8 highlights the fact that the same building blocks are responsible for the formation and chemical structure of the larger PAHs, thus highlighting the repetitive nature of PAH formation chemistry.

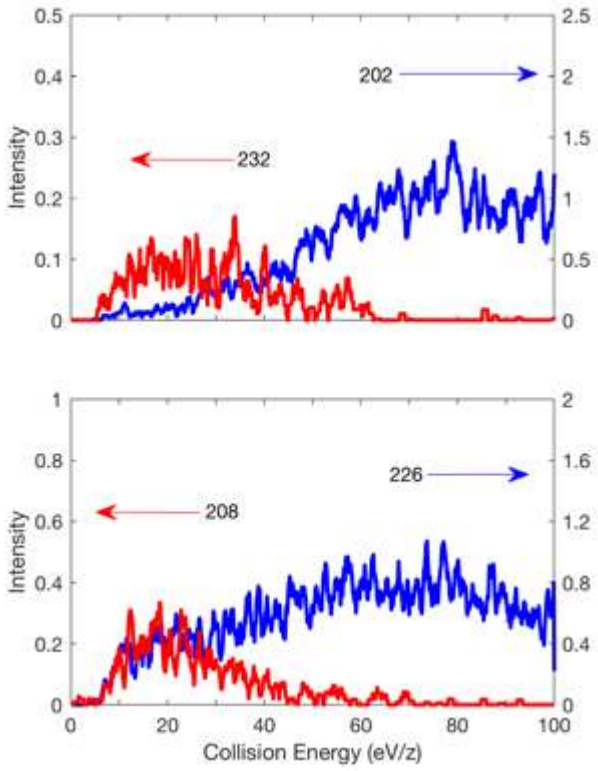

Figure 9: Intensity of *m/z* = 202.078, 208.125, 226.078, and 232.125 fragments formed in the CID of m/z = 434 as function of the collision energy. The stability of the 202 and 226 fragments is indicated, while the respective counter-fragments 232 and 208 dissociate again at higher collision energies, indicating the aliphatic nature of the fragments. Lines represent near-neighbor averages of signal intensities that were recorded in 0.1 eV steps.

Possible $C_{34}H_{26}$ isomers that are consistent with the findings reported in Figs. 8 and 9 are highlighted in Fig. 10. Aliphatically bridged multi-core aromatic structures are highlighted that contain different foundational PAH structures, different lengths of aliphatic bridges, and two- or three aromatic cores. Further complexity can also arise from different isomeric features of the individual foundational PAHs, *i.e.* anthracene *vs.* phenanthrene or pyrene *vs.* fluoranthene. Although not shown here, it should be pointed out that the aliphatic bridges between the multiple aromatic cores allow for interesting three-dimensional configurations in which the aromatic sites are in parallel and appear as π-stacks. While it was shown theoretically that pyrene dimers are not stable enough at flame temperatures to be the starting point of the soot nucleation process,[43] these

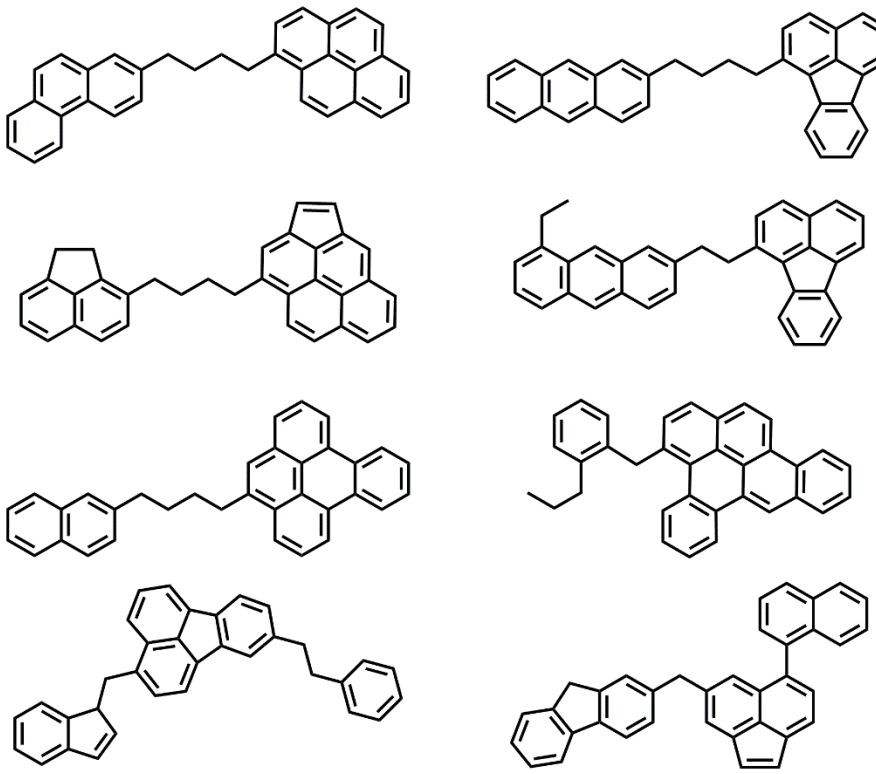

Figure 10. Conceivable $C_{34}H_{26}$ isomers that are consistent with the findings of the tandem mass spectra. The structures consist of dual- and triple core aromatics that are bridged through aliphatic chains.

newly identified covalently bound, three-dimensional multi-core structures could provide the seed for particle nucleation.

Conclusions and Perspectives

Clear experimental evidence for the structural features of alkylated and aliphatically bridged polycyclic aromatic hydrocarbons in hydrocarbon combustion has been provided in the form of flame-sampled tandem mass spectra. This technique offers the advantage that it allows for the identification of reoccurring structural features, while avoiding the difficult task to perform isomer-resolving studies. Alkyl-substituted aromatics were detected that can lose saturated units with up to six C-atoms. This observation is largely consistent with the observations of aliphatic species on soot particles. The mass spectra also revealed the presence of aliphatically bridged PAHs that have enough rotatory degrees of freedom to form three-dimensional structures. Their structural building blocks were identified to be smaller polycyclic aromatic hydrocarbon species. The existence of these structural complicated PAHs had only been hypothesized at this point and the results presented here provide an entire new base for new modeling approaches.[45-46, 70] Especially the modeling procedures described by Violi and coworkers and their implementation into the SNAPS (Stochastic Nanoparticle Simulator) code[32, 75] might already provide a valuable tool with unique capabilities to predict the structural features observed here.

The model development should be guided by the experimental observations. While only two *m/z* ratios (202 and 434) were discussed in detail in this paper, similar data and fragmentation pattern could technically be obtained for any observed ratio, at any given sampling position, and collision energy. Thus, a four-dimensional space can be explored using flame-sampling tandem mass spectrometry in this configuration. However, given the complexity of the observed flame-

sampled mass spectra, it is not considered to be useful to write an individual paper about the fragmentation patterns of every observed *m/z* ratio at any given conditions. Instead, data-science approaches should be developed that automatically explore the available parameter space for re-occurring features in the mass spectra. For example, chemical insights should be obtainable when identifying all parent ions that exhibit the same fragmentation patterns, *e.g.* show the loss of the same alkyl side chain or are based on the same foundational building block. Such automated approaches would allow the identification of repetitive reaction sequences and potentially previously unexplored reaction classes.

The results presented here are consistent with a growth mechanism in which alkylated aromatics, which are formed through reactions of smaller aromatic species and aliphatic hydrocarbons, react to form aliphatically bridged structures. These can get oxidized further to form the energetically more favorable peri-condensed PAH structures that are routinely considered in combustion chemistry models. It should be mentioned that, although the existence of these aliphatic PAHs cannot be explained by the widely-used H-abstraction-C_2H_2-addition mechanism, the HACA reactions are not explicitly ruled out to contribute to PAH growth. For example, pyrene is known to react with C_2H_2 to form the stable $C_{18}H_{10}$ at *m/z* = 226.078 that has been detected throughout this work as a very stable building block. Also, biphenyl-type structures were not explicitly discussed in this paper and therefore the importance of the PAH radical-radical reactions for efficient mass growth were not directly addressed.

Given the fact that weakly bound pyrene dimers are not stable enough at flame temperatures to serve as nucleation particles,[43] it is conceivable that the more stable aliphatically bridged PAHs can serve as a particle seed. The importance of these dual- or triple core PAHs for soot nucleation should be tested in future modeling.

Supporting Information:

Figure S1: Two-dimensional temperature profile of the inverse co-flow flame studied in this paper.

Figure S2: Two-dimensional maps for ion counts in the mass range from 500-600 Da.

Acknowledgements

The experiments were conducted at the Combustion Research Facility, Sandia National Laboratories, Livermore, CA. Support for this work was provided by Sandia National Laboratories under the Laboratory-Directed Research and Development (LDRD) program. Sandia National Laboratories is a multi-mission laboratory managed and operated by National Technology and Engineering Solutions of Sandia, LLC., a wholly owned subsidiary of Honeywell International, Inc., for the U.S. Department of Energy's National Nuclear Security Administration under contract DE-NA0003525. M.A. is supported by the Director, Office of Science, Office of Basic Energy Sciences, of the US Department of Energy under contract no. DE-AC02-05CH11231, through the Gas Phase Chemical Physics Program, Chemical Sciences Division. The authors gratefully acknowledge Paul Fugazzi for technical assistance and Stephen Klippenstein (Argonne National Laboratory) for helpful discussions.

References

1. Frenklach, M. Reaction Mechanism of Soot Formation in Flames. *Phys. Chem. Chem. Phys.* **2002,** *4*, 2028-2037.
2. Wang, H. Formation of Nascent Soot and Other Condensed-Phase Materials in Flames. *Proc. Combust. Inst.* **2011,** *33*, 41-67.
3. Bockhorn, H., *Combustion Generated Fine Carbonaceous Particles*. KIT Scientific Publishing: 2009.
4. McEnally, C. S.; Pfefferle, L. D.; Atakan, B.; Kohse-Höinghaus, K. Studies of Aromatic Hydrocarbon Formation Mechanisms in Flames: Progress Towards Closing the Fuel Gap. *Progr. Energy Combust. Sci.* **2006,** *32*, 247-294.
5. Miller, J. A.; Pilling, M. J.; Troe, J. Unravelling Combustion Mechanisms Through a Quantitative Understanding of Elementary Reactions. *Proc. Combust. Inst.* **2005,** *30*, 43-88.
6. Richter, H.; Howard, J. B. Formation of Polycyclic Aromatic Hydrocarbons and Their Growth to Soot—A Review of Chemical Reaction Pathways. *Progr. Energy Combust. Sci.* **2000,** *26*, 565-608.
7. Hansen, N.; Miller, J. A.; Klippenstein, S. J.; Westmoreland, P. R.; Kohse-Höinghaus, K. Exploring Formation Pathways of Aromatic Compounds in Laboratory-Based Model Flames of Aliphatic Fuels. *Combust. Expl. Shock Waves* **2012,** *48*, 508-515.
8. Hansen, N.; Kasper, T.; Yang, B.; Cool, T. A.; Li, W.; Westmoreland, P. R.; Oßwald, P.; Kohse-Höinghaus, K. Fuel-Structure Dependence of Benzene Formation Processes in Premixed Flames Fueled by C_6H_{12} Isomers. *Proc. Combust. Inst.* **2011,** *33*, 585-592.
9. Ruwe, L.; Moshammer, K.; Hansen, N.; Kohse-Höinghaus, K. Influences of the Molecular Fuel Structure on Combustion Reactions Towards Soot Precursors in Selected Alkane and Alkene Flames. *Phys. Chem. Chem. Phys.* **2018,** *20*, 10780-10795.
10. Hansen, N.; Kasper, T.; Klippenstein, S. J.; Westmoreland, P. R.; Law, M. E.; Taatjes, C. A.; Kohse-Höinghaus, K.; Wang, J.; Cool, T. A. Initial Steps of Aromatic Ring Formation in a Laminar Premixed Fuel-Rich Cyclopentene Flame. *J. Phys. Chem. A* **2007,** *111*, 4081-4092.

11. Melius, C. F.; Colvin, M. E.; Marinov, N. M.; Pit, W. J.; Senkan, S. M. Reaction Mechanisms in Aromatic Hydrocarbon Formation Involving the C_5H_5 Cyclopentadienyl Moiety. *Proc. Combust. Inst.* **1996,** *26*, 685-692.
12. Ruwe, L.; Moshammer, K.; Hansen, N.; Kohse-Höinghaus, K. Consumption and Hydrocarbon Growth Processes in a 2-Methyl-2-Butene Flame. *Combust. Flame* **2017,** *175*, 34-46.
13. Appel, J.; Bockhorn, H.; Frenklach, M. Kinetic Modeling of Soot Formation With Detailed Chemistry and Physics: Laminar Premixed Flames of C_2 Hydrocarbons. *Combust. Flame* **2000,** *121*, 122-136.
14. Frenklach, M.; Wang, H. Detailed Modeling of Soot Particle Nucleation and Growth. *Proc. Combust. Inst.* **1991,** *23*, 1559-1566.
15. Parker, D. S.; Kaiser, R. I.; Bandyopadhyay, B.; Kostko, O.; Troy, T. P.; Ahmed, M. Unexpected Chemistry from the Reaction of Naphthyl and Acetylene at Combustion-Like Temperatures. *Angew. Chem. Int. Ed.* **2015,** *54*, 5421-5424.
16. Constantinidis, P.; Schmitt, H.-C.; Fischer, I.; Yan, B.; Rijs, A. Formation of Polycyclic Aromatic Hydrocarbons From Bimolecular Reactions of Phenyl Radicals at High Temperatures. *Phys. Chem. Chem. Phys.* **2015,** *17*, 29064-29071.
17. Raj, A.; Al Rashidi, M. J.; Chung, S. H.; Sarathy, S. M. PAH Growth Initiated by Propargyl Addition: Mechanism Development and Computational Kinetics. *J. Phys. Chem. A* **2014,** *118*, 2865-2885.
18. Raj, A.; Man, P. L.; Totton, T. S.; Sander, M.; Shirley, R. A.; Kraft, M. New Polycyclic Aromatic Hydrocarbon (PAH) Surface Processes to Improve the Model Prediction of the Composition of Combustion-Generated PAHs and Soot. *Carbon* **2010,** *48*, 319-332.
19. da Silva, G.; Bozzelli, J. W. The C_7H_5 Fulvenallenyl Radical as a Combustion Intermediate: Potential New Pathways to Two-and Three-Ring PAHs. *J. Phys. Chem. A* **2009,** *113*, 12045-12048.
20. Shukla, B.; Koshi, M. A Highly Efficient Growth Mechanism of Polycyclic Aromatic Hydrocarbons. *Phys. Chem. Chem. Phys.* **2010,** *12*, 2427-2437.
21. Shukla, B.; Koshi, M. Comparative Study on the Growth Mechanisms of PAHs. *Combust. Flame* **2011,** *158*, 369-375.

22. Shukla, B.; Koshi, M. A Novel Route for PAH Growth in HACA Based Mechanisms. *Combust. Flame* **2012,** *159*, 3589-3596.
23. Shukla, B.; Susa, A.; Miyoshi, A.; Koshi, M. Role of Phenyl Radicals in the Growth of Polycyclic Aromatic Hydrocarbons. *J. Phys. Chem. A* **2008,** *112*, 2362-2369.
24. Hansen, N.; Cool, T. A.; Westmoreland, P. R.; Kohse-Höinghaus, K. Recent Contributions of Flame-Sampling Molecular-Beam Mass Spectrometry to a Fundamental Understanding of Combustion Chemistry. *Progr. Energy Combust. Sci.* **2009,** *35*, 168-191.
25. Egolfopoulos, F. N.; Hansen, N.; Ju, Y.; Kohse-Höinghaus, K.; Law, C. K.; Qi, F. Advances and Challenges in Laminar Flame Experiments and Implications for Combustion Chemistry. *Progr. Energy Combust. Sci.* **2014,** *43*, 36-67.
26. Michelsen, H. Probing Soot Formation, Chemical and Physical Evolution, and Oxidation: A Review of *in situ* Diagnostic Techniques and Needs. *Proc. Combust. Inst.* **2017,** *36*, 717-735.
27. Qi, F. Combustion Chemistry Probed by Synchrotron VUV Photoionization Mass Spectrometry. *Proc. Combust. Inst.* **2013,** *34*, 33-63.
28. Qi, F.; Yang, R.; Yang, B.; Huang, C.; Wei, L.; Wang, J.; Sheng, L.; Zhang, Y. Isomeric Identification of Polycyclic Aromatic Hydrocarbons Formed in Combustion with Tunable Vacuum Ultraviolet Photoionization. *Rev. Sci. Instrum.* **2006,** *77*, 084101.
29. Homann, K. H. Fullerenes and Soot Formation—New Pathways to Large Particles in Flames. *Angew. Chem. Int. Ed.* **1998,** *37*, 2434-2451.
30. Öktem, B.; Tolocka, M. P.; Johnston, M. V. On-line Analysis of Organic Components in Fine and Ultrafine Particles by Photoionization Aerosol Mass Spectrometry. *Anal. Chem.* **2004,** *76*, 253-261.
31. Öktem, B.; Tolocka, M. P.; Zhao, B.; Wang, H.; Johnston, M. V. Chemical Species Associated With the Early Stage of Soot Growth in a Laminar Premixed Ethylene–Oxygen–Argon Flame. *Combust. Flame* **2005,** *142*, 364-373.
32. Johansson, K.; Lai, J.; Skeen, S.; Popolan-Vaida, D.; Wilson, K.; Hansen, N.; Violi, A.; Michelsen, H. Soot Precursor Formation and Limitations of the Stabilomer Grid. *Proc. Combust. Inst.* **2015,** *35*, 1819-1826.
33. Johansson, K. O.; Dillstrom, T.; Monti, M.; El Gabaly, F.; Campbell, M. F.; Schrader, P. E.; Popolan-Vaida, D. M.; Richards-Henderson, N. K.; Wilson, K. R.; Violi, A. Formation

and Emission of Large Furans and Oxygenated Hydrocarbons from Flames. *Proc. Nat. Acad. Sci.* **2016,** *113*, 8374-8379.

34. Skeen, S. A.; Michelsen, H. A.; Wilson, K. R.; Popolan, D. M.; Violi, A.; Hansen, N. Near-Threshold Photoionization Mass Spectra of Combustion-Generated High-Molecular-Weight Soot Precursors. *J. Aerosol Sci.* **2013,** *58*, 86-102.
35. Schenk, M.; Hansen, N.; Vieker, H.; Beyer, A.; Gölzhäuser, A.; Kohse-Höinghaus, K. PAH Formation and Soot Morphology in Flames of C_4 Fuels. *Proc. Combust. Inst.* **2015,** *35*, 1761-1769.
36. Dijkmans, T.; Djokic, M. R.; Van Geem, K. M.; Marin, G. B. Comprehensive Compositional Analysis of Sulfur and Nitrogen Containing Compounds in Shale Oil Using GC× GC–FID/SCD/NCD/TOF-MS. *Fuel* **2015,** *140*, 398-406.
37. Van de Vijver, R.; Vandewiele, N. M.; Bhoorasingh, P. L.; Slakman, B. L.; Seyedzadeh Khanshan, F.; Carstensen, H. H.; Reyniers, M. F.; Marin, G. B.; West, R. H.; Van Geem, K. M. Automatic Mechanism and Kinetic Model Generation for Gas-and Solution-Phase Processes: A Perspective on Best Practices, Recent Advances, and Future Challenges. *Int. J. Chem. Kin.* **2015,** *47*, 199-231.
38. Stein, S. E.; Fahr, A. High-Temperature Stabilities of Hydrocarbons. *J. Phys. Chem.* **1985,** *89*, 3714-3725.
39. Cain, J. P.; Camacho, J.; Phares, D. J.; Wang, H.; Laskin, A. Evidence of Aliphatics in Nascent Soot Particles in Premixed Ethylene Flames. *Proc. Combust. Inst.* **2011,** *33*, 533-540.
40. Cain, J. P.; Gassman, P. L.; Wang, H.; Laskin, A. Micro-FTIR Study of Soot Chemical Composition—Evidence of Aliphatic Hydrocarbons on Nascent Soot Surfaces. *Phys. Chem. Chem. Phys.* **2010,** *12*, 5206-5218.
41. Faccinetto, A.; Desgroux, P.; Ziskind, M.; Therssen, E.; Focsa, C. High-Sensitivity Detection of Polycyclic Aromatic Hydrocarbons Adsorbed Onto Soot Particles Using Laser Desorption/Laser Ionization/Time-of-Flight Mass Spectrometry: An Approach to Studying the Soot Inception Process in Low-Pressure Flames. *Combust. Flame* **2011,** *158*, 227-239.

42. Faccinetto, A.; Focsa, C.; Desgroux, P.; Ziskind, M. Progress Toward the Quantitative Analysis of PAHs Adsorbed on Soot by Laser Desorption/Laser Ionization/Time-of-Flight Mass Spectrometry. *Environ. Sci. Techn.* **2015,** *49*, 10510-10520.
43. Sabbah, H.; Biennier, L.; Klippenstein, S. J.; Sims, I. R.; Rowe, B. R. Exploring the Role of PAHs in the Formation of Soot: Pyrene Dimerization. *J. Phys. Chem. Lett.* **2010,** *1*, 2962-2967.
44. Totton, T. S.; Misquitta, A. J.; Kraft, M. A Quantitative Study of the Clustering of Polycyclic Aromatic Hydrocarbons at High Temperatures. *Phys. Chem. Chem. Phys.* **2012,** *14*, 4081-4094.
45. Chung, S.-H.; Violi, A. Peri-Condensed Aromatics with Aliphatic Chains as Key Intermediates for the Nucleation of Aromatic Hydrocarbons. *Proc. Combust. Inst.* **2011,** *33*, 693-700.
46. Elvati, P.; Violi, A. Thermodynamics of Poly-Aromatic Hydrocarbon Clustering and the Effects of Substituted Aliphatic Chains. *Proc. Combust. Inst.* **2013,** *34*, 1837-1843.
47. Johansson, K. O.; Dillstrom, T.; Elvati, P.; Campbell, M. F.; Schrader, P. E.; Popolan-Vaida, D. M.; Richards-Henderson, N. K.; Wilson, K. R.; Violi, A.; Michelsen, H. A. Radical–Radical Reactions, Pyrene Nucleation, and Incipient Soot Formation in Combustion. *Proc. Combust. Inst.* **2017,** *36*, 799-806.
48. Cain, J.; Laskin, A.; Kholghy, M. R.; Thomson, M. J.; Wang, H. Molecular Characterization of Organic Content of Soot Along the Centerline of a Coflow Diffusion Flame. *Phys. Chem. Chem. Phys.* **2014,** *16*, 25862-25875.
49. Pascazio, L.; Sirignano, M.; D'Anna, A. Simulating the Morphology of Clusters of Polycyclic Aromatic Hydrocarbons: The Influence of the Intermolecular Potential. *Combust. Flame* **2017,** *185*, 53-62.
50. Schuetz, C. A.; Frenklach, M. Nucleation of Soot: Molecular Dynamics Simulations of Pyrene Dimerization. *Proc. Combust. Inst.* **2002,** *29*, 2307-2314.
51. Lowe, J. S.; Lai, J. Y.; Elvati, P.; Violi, A. Towards a Predictive Model for Polycyclic Aromatic Hydrocarbon Dimerization Propensity. *Proc. Combust. Inst.* **2015,** *35*, 1827-1832.

52. McLafferty, F. W. Tandem Mass Spectrometry (MS/MS): A Promising New Analytical Technique for Specific Component Determination in Complex Mixtures. *Acc. Chem. Res.* **1980,** *13*, 33-39.
53. McLafferty, F. W. Tandem Mass Spectrometry. *Science* **1981,** *214*, 280-287.
54. Ahrens, J.; Keller, A.; Kovacs, R.; Homann, K. H. Large Molecules, Radicals, Ions, and Small Soot Particles in Fuel-Rich Hydrocarbon Flames: Part III: REMPI Mass Spectrometry of Large Flame PAHs and Fullerenes and Their Quantitative Calibration Through Sublimation. *Ber. Bunsen Ges. Phys. Chem.* **1998,** *102*, 1823-1839.
55. Fialkov, A.; Dennebaum, J.; Homann, K.-H. Large Molecules, Ions, Radicals, and Small Soot Particles in Fuel-Rich Hydrocarbon Flames Part V: Positive Ions of Polycyclic Aromatic Hydrocarbons (PAH) in Low-Pressure Premixed Flames of Benzene and Oxygen. *Combust. Flame* **2001,** *125*, 763-777.
56. Griesheimer, J.; Homann, K.-H. Large Molecules, Radicals, Ions, and Small Soot Particles in Fuel-Rich Hydrocarbon Flames: Part II. Aromatic Radicals and Intermediate PAHs in a Premixed Low-Pressure Naphthalene/Oxygen/Argon Flame. *Proc. Combust. Inst.* **1998,** *27*, 1753-1759.
57. Weilmünster, P.; Keller, A.; Homann, K.-H. Large Molecules, Radicals, Ions, and Small Soot Particles in Fuel-Rich Hydrocarbon Flames: Part I: Positive Ions of Polycyclic Aromatic Hydrocarbons (PAH) in Low-Pressure Premixed Flames of Acetylene and Oxygen. *Combust. Flame* **1999,** *116*, 62-83.
58. Hansen, N.; Schenk, M.; Moshammer, K.; Kohse-Höinghaus, K. Investigating Repetitive Reaction Pathways for the Formation of Polycyclic Aromatic Hydrocarbons in Combustion Processes. *Combust. Flame* **2017,** *180*, 250-261.
59. Zhang, W.; Quernheim, M.; Räder, H. J.; Müllen, K. Collision-Induced Dissociation Ion Mobility Mass Spectrometry for the Elucidation of Unknown Structures in Strained Polycyclic Aromatic Hydrocarbon Macrocycles. *Anal. Chem.* **2016,** *88*, 952-959.
60. Arakawa, R.; Kobayashi, M.; Nishimura, T. High-Energy Collision-Induced Dissociation of Small Polycyclic Aromatic Hydrocarbons. *J. Mass Spectrom.* **2000,** *35*, 178-182.
61. Wang, X.; Becker, H.; Hopkinson, A. C.; March, R. E.; Scott, L. T.; Böhme, D. K. Collision-Induced Dissociation of 2- and 3-Dimensional Polycyclic Aromatic

Hydrocarbon Cations in a Modified Ion-Trap Detector. *Int. J. Mass Spectrom. Ion Proc.* **1997,** *161*, 69-76.

62. Pachuta, S. J.; Kenttamaa, H. I.; Sack, T. M.; Cerny, R. L.; Tomer, K. B.; Gross, M. L.; Pachuta, R. R.; Cooks, R. G. Excitation and Dissociation of Isolated Ions Derived From Polycyclic Aromatic Hydrocarbons. *J. Am. Chem. Soc.* **1988,** *110*, 657-665.
63. Shukla, B.; Miyoshi, A.; Koshi, M. Role of Methyl Radicals in the Growth of PAHs. *J. Am. Soc. Mass Spectrom.* **2010,** *21*, 534-544.
64. Raj, A.; Celnik, M.; Shirley, R.; Sander, M.; Patterson, R.; West, R.; Kraft, M. A Statistical Approach to Develop a Detailed Soot Growth Model Using PAH Characteristics. *Combust. Flame* **2009,** *156*, 896-913.
65. Apicella, B.; Carpentieri, A.; Alfè, M.; Barbella, R.; Tregrossi, A.; Pucci, P.; Ciajolo, A. Mass Spectrometric Analysis of Large PAH in a Fuel-Rich Ethylene Flame. *Proc. Combust. Inst.* **2007,** *31*, 547-553.
66. Dobbins, R. A.; Fletcher, R. A.; Benner Jr, B. A.; Hoeft, S. Polycyclic Aromatic Hydrocarbons in Flames, in Diesel Fuels, and in Diesel Emissions. *Combust. Flame* **2006,** *144*, 773-781.
67. Lafleur, A. L.; Taghizadeh, K.; Howard, J. B.; Anacleto, J. F.; Quilliam, M. A. Characterization of Flame-Generated C_{10} to C_{160} Polycyclic Aromatic Hydrocarbons by Atmospheric-Pressure Chemical Ionization Mass Spectrometry with Liquid Introduction via Heated Nebulizer Interface. *J. Am. Soc. Mass Spectrom.* **1996,** *7*, 276-286.
68. Richter, H.; Benish, T. G.; Mazyar, O. A.; Green, W. H.; Howard, J. B. Formation of Polycyclic Aromatic Hydrocarbons and Their Radicals in a Nearly Sooting Premixed Benzene Flame. *Proc. Combust. Inst.* **2000,** *28*, 2609-2618.
69. Senkan, S.; Castaldi, M. Formation of Polycyclic Aromatic Hydrocarbons (PAH) in Methane Combustion: Comparative New Results From Premixed Flames. *Combust. Flame* **1996,** *107*, 141-150.
70. Violi, A. Modeling of Soot Particle Inception in Aromatic and Aliphatic Premixed Flames. *Combust. Flame* **2004,** *139*, 279-287.
71. Holm, A. I.; Johansson, H. A.; Cederquist, H.; Zettergren, H. Dissociation and Multiple Ionization Energies for Five Polycyclic Aromatic Hydrocarbon Molecules. *J. Chem. Phys.* **2011,** *134*, 044301.

72. Poveda, J. C.; Álvarez, I.; Cisneros, C. Molecular Ionization–Dissociation of Fluoranthene at 266 nm: Energetic and Dissociative Pathways. *J. Photochem. Photobio. A: Chem.* **2012,** *230*, 31-37.

73. West, B.; Useli-Bacchitta, F.; Sabbah, H.; Blanchet, V.; Bodi, A.; Mayer, P. M.; Joblin, C. Photodissociation of Pyrene Cations: Structure and Energetics from $C_{16}H_{10}^{+}$ to C_{14}^{+} and Almost Everything in Between. *J. Phys. Chem. A* **2014,** *118*, 7824-7831.

74. Luo, Y.-R., *Handbook of Bond Dissociation Energies in Organic Compounds*. CRC Press LLC: Boca Raton, 2003.

75. Lai, J. Y.; Elvati, P.; Violi, A. Stochastic Atomistic Simulation of Polycyclic Aromatic Hydrocarbon Growth in Combustion. *Phys. Chem. Chem. Phys.* **2014,** *16*, 7969-7979.

Table of Content Graph: